npj | Materials Degradation

www.nature.com/npjmatdeg

ARTICLE OPEN

Accelerated estimation of corrosion rate in supercritical and ultra-supercritical water

David Rodriguez[1] and Dev Chidambaram[1,2]

This study explores a methodology for the determination of the accelerated corrosion rate of candidate materials to be used in advanced supercritical and ultra-supercritical water-based thermal reactors. Electrochemical impedance spectroscopy and electrochemical frequency modulation were used to evaluate the corrosion rates of SAE 316 stainless steel, Nitronic 50, Inconel 718, and Inconel 625 in supercritical water at 530 °C and in ultra-supercritical water at 600 °C. The results were compared to the results of gravimetric studies that were performed to determine the viability of the utilization of electrochemical analyses in supercritical and ultra-supercritical water. For all of the conditions that were tested, results showed that the corrosion rates during electrochemical testing had trends that were similar to the long-term gravimetric results. Thus, the hybrid methodology described in this manuscript can reduce testing times from >1000 h to ~ 10 h.

npj Materials Degradation (2017)1:14 ; doi:10.1038/s41529-017-0006-1

INTRODUCTION

Both nuclear and coal-fired thermal power plants are capable of using supercritical water (SCW) and ultra-supercritical water (USCW). The former is defined as water at an operating temperature and pressure above 375 °C and 22.1 MPa, respectively, and the latter is defined as water at an operating temperature and pressure above 590 °C and 25 MPa, respectively.[1] The benefit of designing power plants that operate with SCW and USCW as the heat transfer media is an increase in the Carnot efficiency. Coal-fired power plants can reach efficiencies of ~ 50% with USCW, while the nuclear industry's proposed reactors that utilize SCW can reach efficiencies of ~ 45%, which is ~ 135% the efficiency of traditional reactors.[2–4]

The properties of SCW necessitate additional evaluations of the structural materials prior to their inclusion in the design of the reactor. An example of the complex nature of SCW is that this fluid behaves as both a gas and a liquid simultaneously.[5] Thus, SCW is characterized as a dense gas, and its corrosion behavior differs from that of liquid water. Due to the complex nature of the environment and the system, studies performed using SCW only have included observations before and after exposure.[6] Since no in situ measurements have been made during typical operating conditions, long-term exposure tests, i.e., months to years, have been required to estimate corrosion rates.[4, 7, 8]

Electrochemical analyses performed by other authors have demonstrated the viability of accelerated corrosion tests, but, to allow such testing, they used conditions that were significantly different from the actual operating conditions of power plants.[9] Botella et al. demonstrated that potentiodynamic polarization scans can be used to evaluate corrosion within a static, 80-mL autoclave that contains SCW.[9] While polarization curves were obtained, various additives were used to improve conductivity, including KCl, HCl, H_2SO_4, and K_2SO_4. Also, this method was limited to a maximum temperature of 400 °C, which does not allow the materials to be tested at the service conditions proposed for supercritical water reactors. Research performed by Beck et al. using supercritical CO_2 as the test environment indicated that the results obtained using direct current were inconsistent and that the use of alternating current produced more reliable results.[10, 11] When electrochemical frequency modulation (EFM) and electrochemical impedance spectroscopy (EIS) were used, the results were more consistent with the values reported in the literature.[10, 11]

SAE stainless steel 316 (SS316), Nitronic 50 (N50), Inconel 625 (I625), and Inconel 718 (I718) were chosen for the tests because they are used extensively in high-temperature power plants.[4, 7, 8, 12–24] This research aims to establish a method for evaluating corrosion rates in pure SCW and to reduce the test time to less than 24 h.

RESULTS

Gravimetric studies

Gravimetric studies were conducted using SS316, N50, I718, and I625 to establish a set of control corrosion rates for comparison with the results obtained from the electrochemical methods used for accelerated corrosion testing. Coupons of SS316 and N50 were exposed to 530 °C SCW and 600 °C USCW for 24 and 96 h to determine the corrosion rate based on the change in mass taken from Rodriguez et al.[21] The corrosion rates of SS316 and N50 were observed to decrease from the time points of 24 and 96 h, so the corrosion rates between these two time points were compared to the electrochemical tests. Table 1 provides the corrosion rates calculated for the steady state conditions of SS316 and N50. In order to determine corrosion rates for I718 and I625, samples were exposed to 530 °C SCW and 600 °C USCW for 24, 96 and 200 h. The average corrosion rate was used for I718 and I625 after 200 h of exposure, because both have been observed to exhibit mass loss and mass gain. Longer exposure times were necessary to obtain accurate results because the rates of mass gain for I718 and I625 were slower than those for N50 and SS316. Based on the values for

[1]Materials Science and Engineering, University of Nevada, Reno, 1664 N. Virginia St., Reno, NV 89557-0388, USA and [2]Nevada Institute for Sustainability, University of Nevada, Reno, 1664 N. Virginia St., Reno, NV 89557-0388, USA
Correspondence: Dev Chidambaram (dcc@unr.edu)

Received: 15 October 2016 Revised: 3 January 2017 Accepted: 21 January 2017
Published online: 21 August 2017

the corrosion rates presented in Table 1, it is apparent that the most corrosion resistant material under these testing conditions was I625, and it was followed by I718, SS316, and N50 in that order. The mass gain data for the Inconel samples compared favorably with data reported by other authors for tests conducted longer than 400 h in SCW.[4, 25]

Electrochemical frequency modulation

While EFM is a relatively new technique, it has been utilized successfully to determine corrosion rates for materials in various environments.[10, 11, 26–28] EFM applies an alternating current that allows non-destructive electrochemical analysis, making it possible to monitor corrosion as a function of time. The perturbation signals, i.e., two base frequencies applied simultaneously, result in current readings at additional harmonic and intermodulation frequencies.[28] The two base frequencies are referred to as ω_1 and ω_2. On the basis of the constructive interference of these signals, it has been observed that harmonic frequencies will occur at multiples of 1, 2, and 3 of each base frequency (i.e., ω_1, ω_2, $2\omega_1$, $2\omega_2$, $3\omega_1$, and $3\omega_2$).[21] As a result of the constructive and destructive interference of the base signals, intermodulation frequencies are known to occur at the values of $\omega_2 \pm \omega_1$, $2\omega_2 \pm \omega_1$, and $\omega_2 \pm 2\omega_1$.[28] In this study, the base frequencies applied to the samples were 20 and 50 mHz, which created harmonics and intermodulation frequencies at 10, 30, 40, 60, 70, 80, 90, 100, 120 and 150 mHz. Using the values of the current at these frequencies, an overall corrosion current was calculated using Eq. (1).[28]

$$i_{corr} = \frac{i^2_{\omega 1,\omega 2}}{2\times\sqrt{8\times i_{\omega 1,\omega 2}\times i_{2\omega 1\pm\omega 2} - 3\times i^2_{\omega 2\pm\omega 1}}}, \quad (1)$$

where $i_{\omega 1,\omega 2}$ is the average of the current densities at frequencies of 20 and 50 mHz, $i_{2\omega 2\pm\omega 1}$is the average of the current densities at frequencies of 10, 80, 90, and 120 mHz, and $i_{\omega 2\pm\omega 1}$ is the average of the current densities at frequencies of 30 and 70 mHz. By using the average values of the harmonic current densities in Eq. (1), a corrosion current value can be calculated and used with Faraday's Law to calculate the corresponding corrosion rate.[28] Surfaces of materials exposed to SCW and USCW have been previously studied using SEM, EBSD, Raman, XRD and XPS and results have shown the formation of a uniform oxide layer on the surface. Therefore, it is reasonable to assume that the exposure of these materials to SCW and USCW will result in uniform corrosion.[4, 21, 22, 29] The values of atomic mass and equivalents exchanged for austenitic alloys were 55.85 and 2, respectively. These values correspond to Fe, which has been reported in literature to be the main corroding species in SS316.[4, 7, 8, 12–20] Calculations of the corrosion rates of Inconel alloys were performed using the values of 58.69 for *a* and 2 for n since Ni has been identified as the primary corroding element.[4, 6, 15, 29–32]

The intermodulation spectra obtained from SS316 exposed to SCW at 530 °C and USCW at 600 °C are shown in Fig. 1a and 1b, respectively. An example of the procedure used in the calculation of the corrosion rates of SS316 is presented, and the data from the electrochemical tests performed on N50, I718, and I625 are presented in Supplementary Fig. S1. The resulting corrosion currents for SS316 exposed to 530 °C SCW and 600 °C USCW were calculated using Eq. (1), and they were 2.17 and 4.11 μA/cm^2, respectively. Using the equations above and the values of the current at the harmonics mentioned, the resulting corrosion rates were found to be 62.8 and 118 μg/cm^{2}day for 530 °C SCW and 600 °C USCW, respectively. These values were compared with the values obtained from the exposure testing in conjunction with gravimetric methods to determine corrosion rates, and they are used in a subsequent section to assess the viability of the EFM technique. Supplementary Figure S2 shows the progression of the corrosion rate of SS316 as a function of time when it was exposed to 530 °C SCW. After obtaining the data in Supplementary Fig. S2, subsequent electrochemical tests were performed after an exposure time of 24 h to ensure that the data were obtained in a stable region.

The last parameters calculated from Fig. 1a and 1b were the cathodic and anodic Tafel constants. These parameters were calculated with Eqs (2) and (3) below, which were taken from

Table 1. Summary of corrosion rate values for gravimetric studies: Corrosion rates for SS316, N50, I718 and I625 in supercritical and ultra-supercritical water for gravimetric studies

Alloy	Temperature (° C)	Corrosion Rate (μg/cm^{2}day)	Error ± (μg/cm^{2}day)
SS316	530	98.8	17.4
	600	187	2.90
N50	530	131	3.20
	600	271	9.00
I718	530	38.2	4.89
	600	46.4	6.20
I625	530	14.3	2.40
	600	33.4	9.50

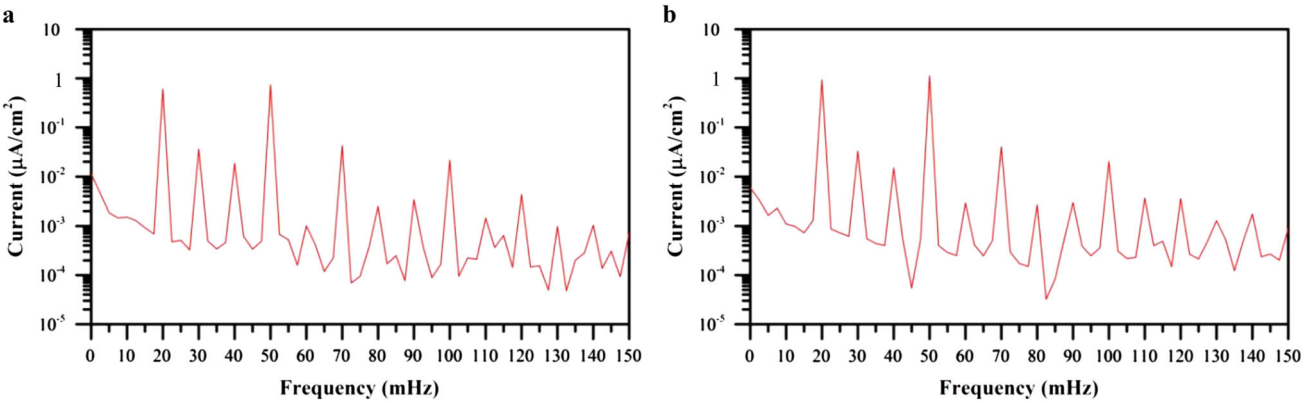

Fig. 1 Intermodulation spectrum from electrochemical frequency modulation for SS316: **a** exposed to supercritical water at 530 °C, **b** exposed to ultra-supercritical water at 600 °C

Rosch et al. [28]

$$\beta_a = \frac{i_{\omega1,\omega2} \times U}{i_{\omega1,\omega2} + \sqrt{8 \times i_{\omega1,\omega2} \times i_{2\omega1 \pm \omega2} - 3 \times i^2_{\omega2 \pm \omega1}}} \quad (2)$$

$$\beta_c = \frac{i_{\omega1,\omega2} \times U}{-i_{\omega1,\omega2} + \sqrt{8 \times i_{\omega1,\omega2} \times i_{2\omega1 \pm \omega2} - 3 \times i^2_{\omega2 \pm \omega1}}}, \quad (3)$$

where U is the applied potential, β_a is the anodic Tafel constant, and β_c is the cathodic Tafel constant.

When exposed to 530 °C SCW, SS316 was found to have β_a and β_c values of 0.383 and 0.873 V/decade, respectively. For SS316 exposed to 600 °C USCW, the anodic and cathodic Tafel constants were calculated as 0.468 and 0.875 V/decade, respectively. These values are used in the next section to calculate the corrosion rate using EIS.

Electrochemical impedance spectroscopy

The non-destructive behavior of AC analysis allows collaborative electrochemical tests to be run in series. When the EFM test was completed, a EIS test was run as a secondary test to determine the validity of monitoring the corrosion rate using electrochemical methods. Previous studies have indicated that two distinct oxide layers will form on austenitic steels when they are exposed to SCW and USCW. The layer formed on the surface of the alloy is a porous, chromium-rich spinel ($FeCr_2O_4$) and Cr_2O_3, which allows the diffusion of iron from the surface of the alloy through the film. The diffusing iron forms magnetite (Fe_3O_4) on the chromium-rich layer, and the magnetite is oxidized to form hematite (Fe_2O_3).[4, 7, 8, 12–22] For Inconel alloys, it has been observed that oxide layers form in a similar manner with some differences in the surface chemistry. On the surfaces of Inconel alloys, Cr compounds, specifically $NiCr_2O_4$ and Cr_2O_3, form porous layers that allow Ni and Fe to diffuse to the surface and form $NiFe_2O_4$.[4, 6, 15, 29–32] Based on this surface analysis, an equivalent circuit was constructed to represent all alloys tested within this study, and it is shown in Fig. 2a. The outer oxide layer was modeled with a simple RC circuit, while the inner oxide layer was observed to be porous, which allows for the diffusion of alloy components to the surface.[15–17] Since the outer oxide layer has been reported to form as a result of diffusion of the base material through the inner layer, a Warburg element through a porous medium was incorporated to account for this behavior.[17] The elements used in this circuit included a resistor for solution resistance, a constant phase element for the alumina washers, and a resistor and a capacitor for the outer oxide layer. The inner oxide layer was modeled using a resistor, capacitor, and a Warburg element through a porous medium, which, in this case, represented the porosity that was indicative of the chromium-rich spinel. The important elements are labeled R_p, and the sum of these resistances was used in the calculation of the corrosion rate. The corrosion current was calculated using the Stern–Geary equation with the proportionality constant that was calculated

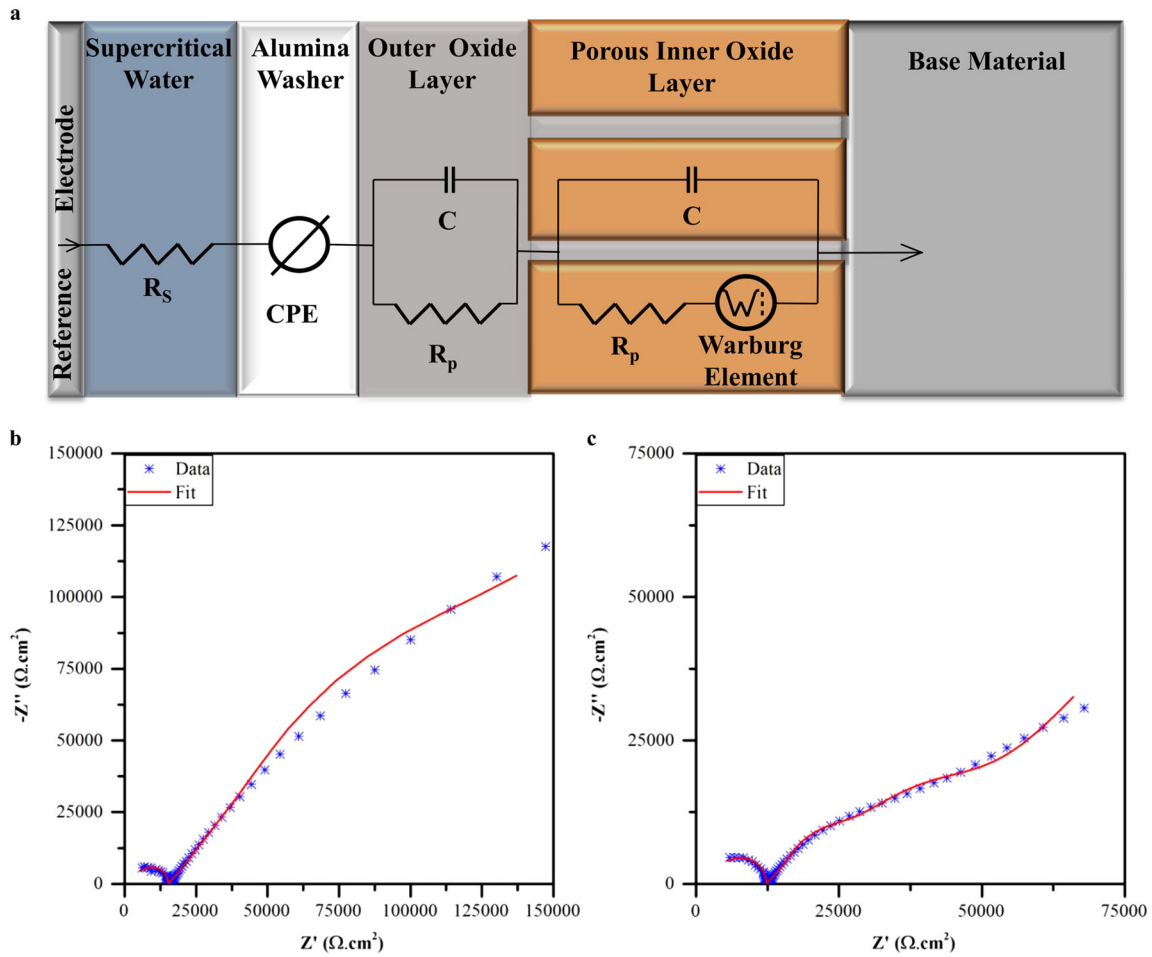

Fig. 2 Electrochemical impedance spectroscopy: **a** Equivalent circuit used to model the corrosion behavior for electrochemical impedance spectroscopy data, **b** Nyquist plot for SS316 exposed to supercritical water at 530 °C, **c** Nyquist plot for SS316 exposed to ultra-supercritical water at 600 °C

using the Tafel constants obtained from the EFM experiments. Using the sum of the resistances, R_p, from the equivalent circuit applied to Fig. 3b and 3c, the current density was calculated to be 2.48 μA/cm^2 for SS316 exposed to 530 °C SCW and 4.73 μA/cm^2 for SS316 exposed to 600 °C USCW. Then, the calculated current density values were used with Faraday's Law, and a corrosion rate was calculated with the assumption that Fe had the primary influence on the corrosion rate for this system. The resulting corrosion rates were calculated as 71.9 and 137 μg/cm^{2}day for 530 °C SCW and 600 °C USCW, respectively. The resultant Nyquist plots for N50, I718 and I625 are presented in Supplementary Fig. S3.

DISCUSSION

Corrosion rates of materials in SCW and USCW, at conditions that are representative of the proposed operational parameters, have been exclusively determined using long-term exposure testing.[4, 9, 16, 21, 25]

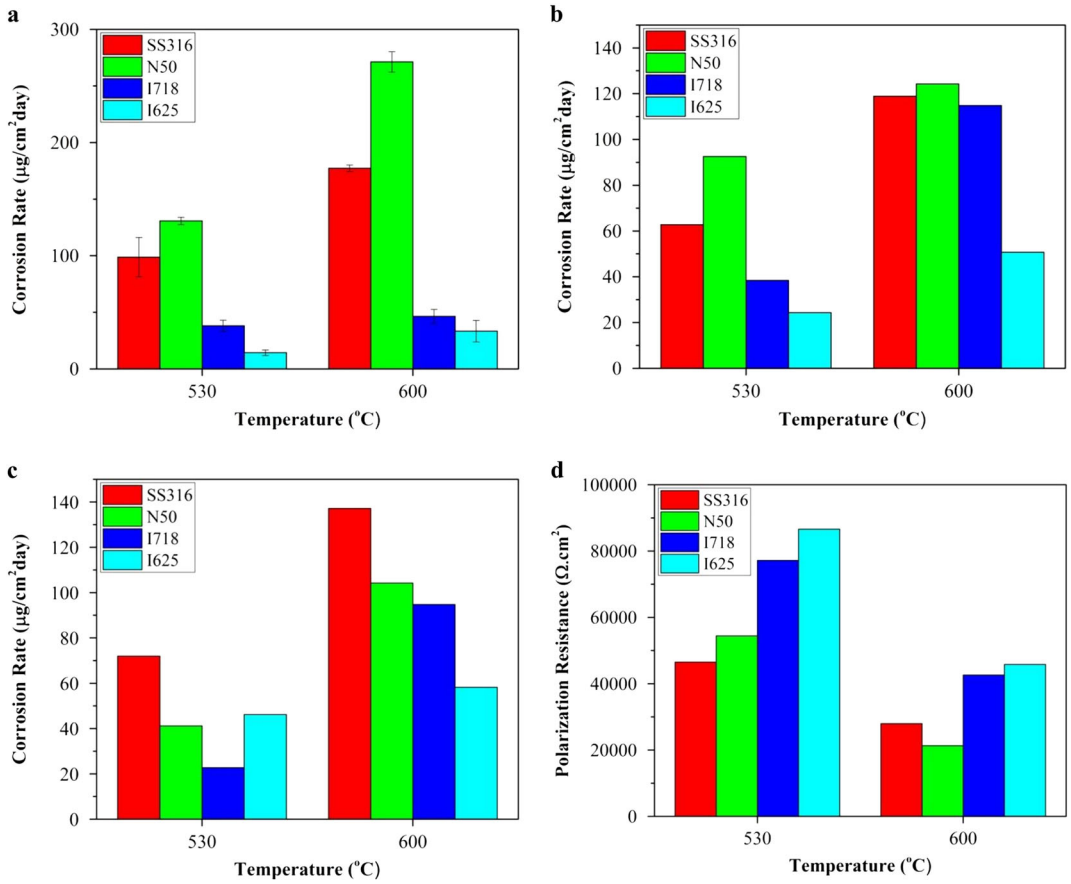

Fig. 3 Quantification of corrosion behavior: Summary of **a** corrosion rates calculated from exposure testing, **b** corrosion rates calculated from electrochemical frequency modulation, **c** corrosion rates calculated from electrochemical impedance spectroscopy, **d** polarization resistance values from electrochemical impedance spectroscopy for SS316, N50, I718 and I625 exposed to supercritical water at 530 °C and ultra-supercritical water at 600 °C

Table 2. Comparison of corrosion rates obtained from electrochemical and gravimetric studies: Corrosion rate values of SS316, N50, I718 and I625 in supercritical and ultra-supercritical water as determined from gravimetric studies, EFM and EIS

		EFM		EIS			Exposure	
Alloy	Temperature (°C)	icorr (μA/cm^2)	Corrosion rate (μg/cm^{2}day)	Rp (kΩ.cm^2)	icorr (μA/cm^2)	Corrosion rate (μg/cm^{2}day)	Corrosion rate (μg/cm^{2}day)	Error ± (μg/cm^{2}day)
SS316	530	2.17	62.8	46.5	2.49	71.9	98.8	17.4
	600	4.11	118	27.9	4.74	137	187	2.90
N50	530	3.20	92.5	54.4	1.42	41.2	131	3.20
	600	4.29	124	21.3	3.60	104	271	9.00
I718	530	1.26	38.5	77.1	0.75	22.8	38.2	4.89
	600	3.78	115	42.6	3.12	94.7	46.4	6.20
I625	530	0.80	24.4	86.6	1.52	46.2	14.3	2.40
	600	1.67	50.7	45.8	1.91	58.2	33.4	9.50

As shown in Table 2, the corrosion rates obtained for the gravimetric studies compare favorably with the corrosion rates calculated from the EFM and EIS methods used in this study. As shown in Fig. 3, while there are some differences in the values for the corrosion rates calculated utilizing the electrochemical methods and compared to exposure testing, the ranking of the materials based on corrosion resistance determined using the electrochemical methods duplicated the trends that were observed from the exposure testing results. By using EFM testing, it was found that N50 had the highest corrosion rate, and it was followed by SS316, I718, and I625 in descending order of corrosion rates. This trend was consistent with our observations during the exposure tests for these materials. While EIS did not exhibit a similar trend for all cases, this can be explained by the reliance on the Tafel constants from the EFM method for the calculation of the corrosion rate from the data obtained using the EIS technique. To eliminate this potential source of error, the polarization resistances can be used as a general way of presenting the corrosion resistance of materials, with higher values correlating to greater corrosion resistance. The polarization resistances are presented in Fig. 3d. It can be observed that the polarization resistance values followed the trend established in the gravimetric studies and EFM sections. As with the EFM study, it can be observed that polarization resistance values calculated from EIS corroborated that I625 was the most resistant to corrosion, and it was followed by I718, SS316 and N50. An additional potential source for the deviations observed in electrochemical testing could be the differences in finding the instantaneous corrosion rate using electrochemical methods, while exposure testing calculates an average corrosion rate.

Previous gravimetric studies have demonstrated that austenitic alloys have higher mass gain rates than Inconel alloys.[4, 25, 33] The trend established in the literature is that increasing Ni content results in a decreased mass gain rate.[4, 25, 33] The experiments conducted to determine the mass gain rate for these materials were performed at exposure times ranging from 96 to 3000 h.[4, 21, 25, 33] Through the use of EFM, corrosion rates were calculated that duplicated the trend established in the literature, i.e., that increasing Ni content results in lower corrosion. While the corrosion rates calculated through the use of EIS did not follow this trend, the values for polarization resistances were comparable to the trends in the literature. The electrochemical techniques used in this manuscript were used to determine corrosion rates in 24 h that correlate to reported trends that were established in long-term exposure tests. Decreasing the time to 24 h results in significant time savings, ranging from 25 to 99%, and this allows higher throughput during the preliminary screening of materials.

The EFM and EIS techniques provided consistent data in the determination of corrosion rates. When the results of the exposure testing were compared, the corrosion rates for EFM and EIS were found to be within a factor of ~ 3.2. On the basis of the results presented in this work, using EFM to determine corrosion rates established a similar trend of corrosion rates for materials tested by gravimetric methods. These results demonstrated that, by using EFM, a series of corrosion rates can be determined in less than 24 h. This is a significantly shorter time than that required by traditional gravimetric methods, which require weeks or months.[4, 21, 22, 25, 32] While EIS did not provide corrosion rates as accurate as the EFM method, the values obtained for the polarization resistance followed the trend established by EFM and exposure testing. Since the data presented here follow the trends of long-term exposure testing, it is recommended that this method be used for preliminary screening of candidate materials rather than as a substitute for long-term testing for full service life because there may be other long-term effects that can change the corrosion behavior.

METHODS

The composition of SS316 used in this study in wt% was (0.03% C, 2% Mn, 0.05% P, 0.03% S, 0.75% Si, 18% Cr, 14% Ni, 0.1% N, 3% Mo, 0.3% V, 0.3% Nb, and the balance was Fe). The composition of Nitronic 50 in wt% was (0.03% C, 4.89% Mn, 0.02% P, 0.001% S, 0.49% Si, 21.26% Cr, 12.18% Ni, 0.28% N, 2.1% Mo, 0.14% V, 0.18% Nb, and the balance was Fe). The composition of Inconel 718 in wt% was (0.05% C, 0.05% Mn, 0.008% P, 0.0004% S, 0.07% Si, 18.25% Cr, 0.56% Al, 2.89% Mo, 0.02% Cu, 5.05% Nb, 0.01% Ta, 1.01% Ti, 0.06% Co, 19.83% Fe, and the balance was Ni). The composition of Inconel 625 in wt% was (0.02% C, 0.04% Mn, 0.005% P, 0.001% S, 0.2% Si, 21.32% Cr, 0.16% Al, 8.68% Mo, 3.36% Nb, 0.2% Ti, 0.04% Co, 4.62% Fe, and the balance was Ni). The experimental coupons were polished to a one micron finish prior to use in the supercritical water loop.

The autoclave pressure was held at 27 MPa during all of the tests. The temperature was monitored using a type K thermocouple. The supercritical water loop test solution was 18 MΩ deionized water that was deaerated continuously with nitrogen to maintain a dissolved oxygen content of less than 50 ppb throughout the operation. Evaluation of the corrosion using accelerated and gravimetric methods were performed in a test solution at temperatures of 530 and 600 °C.

The dimensions of the coupons in the gravimetric studies were 2.2 × 2.5 × 0.625 cm. The SS316 and N50 samples were exposed to the test temperatures for 24 and 96 h. All exposure testing experiments were conducted using duplicate samples. The I718 and I625 samples were exposed to the test temperatures for 24, 96, and 200 h. Prior to the determination of mass, each coupon was dried in a low vacuum chamber for 1 day. Mass was determined with an Ohaus Adventurer SL model AS214 scale that had a resolution of 100 µg before and after exposure to the conditions of each experiment.

All samples for the electrochemical tests were laser cut into coupons that measured 0.3 × 0.9 × 4.5 cm with two 0.5-cm holes to secure the samples. Electrochemical tests were conducted using single sample. The samples were held in place using an assembly of washers, nuts, and bolts that were made of alumina to ensure electrical insulation from the autoclave. The washers used in these experiments were 1.1 mm thick, and they were used to maintain a specific distance between the counter, reference, and working electrodes. All potentials were measured with respect to a silver wire reference electrode. The electrochemical tests were performed using a REF 600 model potentiostat supplied by Gamry Instruments, Inc. Gamry Framework version 4.1 was used to control the potentiostat, and Gamry's ECHEM analyst version 6.25 was used to analyze the data. EFM testing was performed using a signal amplitude of 25 mV rms vs. the open-circuit potential at frequencies of 20 and 50 mHz. EIS measurements were conducted in the frequency range from 100 kHz to 10 mHz with an amplitude of 25 mV r.m.s. vs. the open-circuit potential.

ACKNOWLEDGEMENTS

This study was supported by the Nuclear Regulatory Commission (NRC) under awards NRC-HQ-11-G-38-0039 and NRC-38-10-949. D.R. is supported under NRC Fellowship award. Nancy Hebron-Isreal serves as the grants program officer for the NRC awards. The supercritical water loop was funded in part by the Department of Energy through a Nuclear energy grant: DE-NE0000454. Kenny Osborne serves as the program manager for the DOE award.

AUTHOR CONTRIBUTIONS

D.R. and D.C. designed the experiments; D.R. performed the experiments. All the authors discussed the results. D.R. and D.C. wrote the paper and all the authors read and commented on the manuscript.

ADDITIONAL INFORMATION

Supplementary Information accompanies the paper on the *npj Materials Degradation* website (doi:10.1038/s41529-017-0006-1).

Competing interests: The authors declare that they have no competing financial interests.

Publisher's note: Springer Nature remains neutral with regard to jurisdictional claims in published maps and institutional affiliations.

REFERENCES

1. Phillips, J. & Wheeldon, J. in *Advances in Materials Technology for Fossil Power Plants: Proceedings of the Sixth International Conference, 2010* (eds Gandy, D., Shingledecker, J. & Viswanathan, R.) 65–71 (ASM International, 2011).
2. Cebrucean, D., Cebrucean, V. & Ionel, I. CO2 capture and storage from fossil fuel power plants. *Energy Procedia* **63**, 18–26 (2014).
3. Dobashi, K., Kimura, A., Oka, Y. & Koshizuka, S. Conceptual design of a high temperature power reactor cooled and moderated by supercritical light water. *Ann Nucl Energy* **25**, 487–505 (1998).
4. Allen, T. R. et al. in *Comprehensive Nuclear Materials*, Vol. 5 (ed. Konings, R.) Ch. 12 (Elsevier, 2012)
5. Kritzer, P. Corrosion in high-temperature and supercritical water and aqueous solutions: a review. *J. Supercrit. Fluids* **29**, 1–29 (2004).
6. Guzonas, D. A. & Cook, W. G. Cycle chemistry and its effect on materials in a supercritical water-cooled reactor: a synthesis of current understanding. *Corros. Sci.* **65**, 48–66 (2012).
7. Ampornrat, P. & Was, G. S. Oxidation of ferritic–martensitic alloys T91, HCM12A and HT-9 in supercritical water. *J. Nucl. Mater.* **371**, 1–17 (2007).
8. Cao, G., Firouzdor, V. & Allen, T. in *Environmental Degradation of Materials in Nuclear Power Systems:Water Reactors* Vol. 3 (eds Busby, J., Ilevbare, G. & Andersen, P.) 1923-1936 (Wiley, 2012).
9. Botella, P., Cansell, F., Jaszay, T., Frayret, J. P. & Delville, M. H. Experimental set-up for electrochemical measurements in hydrothermal sub- and supercritical oxidation: polarization curves, determination of corrosion rates and evaluation of the degradability of reactors during hydrothermal treatments of aqueous wastes. *J. Supercrit. Fluids* **26**, 157–167 (2003).
10. Beck, J., Fedkin, M. & Lvov, S. N. Electrochemical corrosion measurements in supercritical carbon dioxide - water systems with and without membrane coating. *ECS Trans* **50**, 315–334 (2013).
11. Beck, J. et al. In Situ electrochemical corrosion measurements of carbon steel in supercritical CO2 using a membrane-coated electrochemical probe. *ECS Trans* **45**, 39–50 (2013).
12. Was, G. S. et al. Corrosion and stress corrosion cracking in supercritical water. *J. Nucl. Mater.* **371**, 176–201 (2007).
13. Sun, M., Wu, X., Zhang, Z. & Han, E. H. Oxidation of 316 stainless steel in supercritical water. *Corros. Sci.* **51**, 1069–1072 (2009).
14. Tan, L. & Allen, T. R. Localized corrosion of magnetite on ferritic–martensitic steels exposed to supercritical water. *Corros. Sci.* **51**, 2503–2507 (2009).
15. Tan, L., Ren, X., Sridharan, K. & Allen, T. R. Corrosion behavior of Ni-base alloys for advanced high temperature water-cooled nuclear plants. *Corros. Sci.* **50**, 3056–3062 (2008).
16. Bischoff, J. & Motta, A. T. Oxidation behavior of ferritic–martensitic and ODS steels in supercritical water. *J. Nucl. Mater.* **424**, 261–276 (2012).
17. Bischoff, J. et al. Corrosion of ferritic–martensitic steels in steam and supercritical water. *J. Nucl. Mater.* **441**, 604–611 (2013).
18. Gómez-Briceño, D., Blázquez, F. & Sáez-Maderuelo, A. Oxidation of austenitic and ferritic/martensitic alloys in supercritical water. *J. Supercrit. Fluids* **78**, 103–113 (2013).
19. Guzonas, D. & Novotny, R. Supercritical water-cooled reactor materials—Summary of research and open issues. *Prog. Nuclear Energy* **77**, 361–372 (2014).
20. Novotny, R. et al. Stress corrosion cracking susceptibility of austenitic stainless steels in supercritical water conditions. *J. Nucl. Mater.* **409**, 117–123 (2011).
21. Rodriguez, D. & Chidambaram, D. Oxidation of stainless steel 316 and Nitronic 50 in supercritical and ultrasupercritical water. *Appl. Surf. Sci.* **347**, 10–16 (2015).
22. Rodriguez, D., Merwin, A. & Chidambaram, D. On the oxidation of stainless steel alloy 304 in subcritical and supercritical water. *J. Nucl. Mater.* **452**, 440–445 (2014).
23. Karmiol, Z. & Chidambaram, D. Comparison of performance and oxidation of nitronic-50 and stainless steel 316 in subcritical and supercritical water environments. *MMTA* **47**, 2498–2508 (2016).
24. Schulenberg, T. et al. European supercritical water cooled reactor. *Nucl. Eng. Des.* **241**, 3505–3513 (2011).
25. Guzonas, D. A., Wills, J., Do, T. & Michel J. in *13th International Conference on Environmental Degradation of Materials in Nuclear Power Systems 2007* Vol. 3 (eds Canadian Nuclear Society) 1250-1261 (Canadian Nuclear Society, 2007).
26. Beese, P. et al. Monitoring of anaerobic microbially influenced corrosion via electrochemical frequency modulation. *Electrochim. Acta* **105**, 239–247 (2013).
27. Han, L. & Song, S. A measurement system based on electrochemical frequency modulation technique for monitoring the early corrosion of mild steel in seawater. *Corros. Sci.* **50**, 1551–1557 (2008).
28. Bosch, R. W., Hubrecht, J., Bogaerts, W. F. & Syrett, B. C. Electrochemical frequency modulation: a new electrochemical technique for online corrosion monitoring. *Corrosion* **57**, 60–70 (2001).
29. Merwin, A., Rodriguez, D. & Chidambaram, D. Oxidation of superalloys in supercritical water. *ECS Trans* **58**, 15–24 (2014).
30. Huang, X. & Guzonas, D. Characterization of Ni–20Cr–5Al model alloy in supercritical water. *J. Nucl. Mater.* **445**, 298–307 (2014).
31. Fujii, T., Sue, K. & Kawasaki, S. Effect of pressure on corrosion of Inconel 625 in supercritical water up to 100 MPa with acids or oxygen. *J. Supercrit. Fluids* **95**, 285–291 (2014).
32. Ren, X., Sridharan, K. & Allen, T. R. Corrosion behavior of alloys 625 and 718 in supercritical water. *Corrosion* **63**, 603–612 (2007).
33. Jiao, Y., Zheng, W., Guzonas, D. A., Cook, W. G. & Kish, J. R. Effect of thermal treatment on the corrosion resistance of Type 316L stainless steel exposed in supercritical water. *J. Nucl. Mater.* **464**, 356–364 (2015).